scientific reports

Check for updates

OPEN

Bigger is faster in the adaptive immune response

Jannatul Ferdous[1,6]✉, G. Matthew Fricke[1,2,6], Judy L. Cannon[3,6] & Melanie E. Moses[1,4,5,6]

Zoonotic pathogens represent a growing global risk, yet the speed of adaptive immune activation across mammalian species remains poorly understood. Despite orders-of-magnitude differences in size and metabolic rate, we show that the time to initiate adaptive immunity is remarkably consistent across species. To understand this invariance, we analyse empirical data showing how the numbers and sizes of lymph nodes scale with body mass, finding that larger animals have both more and larger lymph nodes. Using scaling theory and our mathematical model, we show that larger lymph nodes enable faster search times, conferring an advantage to larger animals that otherwise face slower biological times. This enables mammals to maintain, or even accelerate, the time to initiate the adaptive immune response as body size increases. We validate our analysis in simulations and compare to empirical data.

Mammal body masses range over 8 orders of magnitude, from the 2 g bumblebee bat to the 15,0000 kg blue whale. Most biological processes slow with increasing body size, following a quarter-power scaling law[1–3]. While the cause of quarter-power scaling is debated[4–6], empirical observations consistently show that smaller mammals have faster physiology and life history, and larger mammals have slower rates over longer times[7–10]. For example, humans who are 2,500 times larger than mice, are predicted to have heart rates, breathing rates, and gestation times that are 7 times slower than mice; actual values are 7 to 14 times slower, within a factor of 2 of the prediction[7,11,12].

Despite the orders of magnitude increase in size and the slower metabolic rate of humans, the initial detection of the primary T cell response time in humans is indistinguishable from that of mice (Table 1). Large animals clearly require that the immune response remain fast enough to counter exponentially growing pathogens. However, the mechanisms that allow larger mammals to respond as quickly as smaller, metabolically faster, ones remain unclear. The immune response proceeds through a sequence of interdependent steps, each reliant on the preceding one (Fig. 1). Efficient scaling requires that none of these steps becomes a bottleneck.

Lymph nodes (LNs) play a central role in this process. LN are the organs in which antigens indicative of infection are first recognized by T cells capable of mounting a pathogen-specific defense. We propose that the scaling rules governing the number and size of LNs help explain why two critical steps, transport of antigens to LNs (step 2) and T cell contact with antigens carried by DCs within LN (steps 3–5), remain fast across body sizes.

Our analysis considers a simplified model of immune response. We primarily focus on Fig. 1, steps 3 - 5 within LNs. We focus on generic LN search dynamics without distinguishing $CD4^+/CD8^+$ specific mechanisms, because no evidence suggests T cell activation dynamics are different between $CD4^+/CD8^+$ T cells. We simplify the adaptive immune response to generalized steps beginning with infection at peripheral tissue sites (Fig. 1, step 1) where pathogens can establish and replicate. To initiate the adaptive immune response, dendritic cells (DCs) in the tissues activate via Pattern Recognition Receptor signaling to ingest and process antigens produced by pathogens; they then upregulate migration receptors such as CCR7, and migrate via lymphatic vessels to draining LNs (step 2). While different pathogens activate different pathways and subsets of immune cells, such factors are not known to substantially affect the timing of these steps. DCs in LN display antigens (step 3) and naïve T cells move through LNs in search of cognate antigen-bearing DCs (step 4). For simplicity we consider CD8+ T cells that bind and activate (step 5) and then migrate through the blood to the site of infection (step 6), where they kill infected cells displaying cognate antigens (step 7). This simplification of the very complex immune response focuses on CD8+ T cell activation that underlies anti-viral adaptive immunity, and not binding differences to MHC classes governing CD4+ T cell activation or high affinity antibody generation. We focus on the timing of T cell contact with DCs in LNs because this is the initiating event leading to other downstream adaptive immune responses.

[1]Department of Computer Science, The University of New Mexico, Albuquerque, USA. [2]Center for Advanced Research Computing, Albuquerque, USA. [3]Molecular Genetics and Microbiology, The University of New Mexico, Albuquerque, USA. [4]Department of Biology, The University of New Mexico, Albuquerque, USA. [5]Santa Fe Institute, Santa Fe, USA. [6]These authors authors contributed equally to this work: Jannatul Ferdous, G. Matthew Fricke, Judy L. Cannon and Melanie E. Moses. ✉email: jannat@unm.edu

	M. musculus (24 g)	*H. sapiens* (62 kg)
	Flu: 5 d[32,35]	Dengue: 7 d[36]
	Flu: 4–6 d[37]	Flu: 6 d[38]
	Flu: 5–7 d[39]	LCMV: 4–5 d[40]
	HSV: 5–7 d[41,42]	RSV: 7–10 d[43]
	LCMV: 5–7 d[44]	SARS2: 4 d[45,46]
	SARS2: 5–10 d[31]	SARS2: 6 d[47,48]
	SARS2: 7 d[49]	SARS2: 7 d[50,51]
	Staph: 6 d[52]	Staph: 7 d[53,54]
	Staph: 9 d[55]	
n	11	12
Mean	6 d	6 d
Min	4 d	4 d
Max	10 d	10 d

Table 1. Time to Initial Detection of Activated T Cells in Mice and Humans. Data are rounded to the nearest day (d). *n* is the number of published studies. Means are calculated from the midpoint of each reported range. Minimum and maximum values reflect the full span of reported values across all studies. (SARS2: Severe acute respiratory syndrome coronavirus 2; LCMV: Lymphocytic choriomeningitis virus; HSV: Herpes simplex virus; RSV: Respiratory syncytial virus).

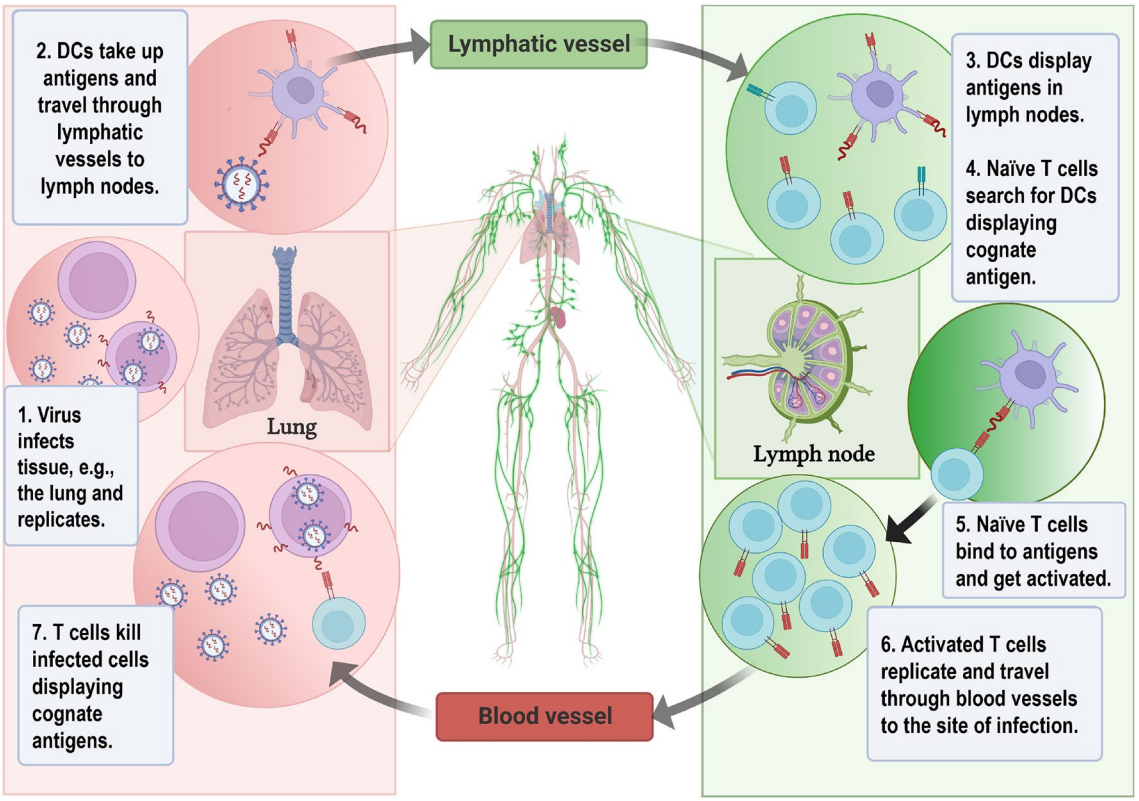

Fig. 1. Simplified schematic of T cell activation by DCs. 1) A pathogen infects tissue, e.g., the lung. 2) DCs deliver the captured antigens from tissue through lymphatic vessels to draining LNs. 3) DCs display antigens in the LN. 4) Naïve T cells search for cognate antigens presented on the surface of DCs. 5) T cell receptors recognize cognate antigens upon encountering an antigen-bearing DC and become activated upon receiving the necessary activation signal (step 5). 6) Activated CD8+ T cells proliferate exponentially, and transform into cytotoxic T cells (CTLs) that travel through the bloodstream to the inflamed, infected area. 7) CTLs kill infected cells that display cognate antigens. We model the timing of search and activation in steps 4 and 5, where the adaptive immune response is initiated; the timing of this process depends on LN size.

Scaling Context: A well-established scaling relationship is that organ size typically scales linearly across animals. For example, the heart, liver, and kidney are 1,000 times larger in animals weighing 1000 times more[4]. We show that LNs deviate from this pattern and argue that the non-linear allocation of LN size and number contributes to the invariance of the immune system response time. We establish scaling relationships for how LN volume, and DC and T cell populations scale with body mass, and then we analyze how those scaling relationships determine how quickly the first T cells come into contact with DC carrying cognate antigens in LN.

The effect of LN scaling on immune response has been studied previously[13–16]. Of particular relevance here, Perelson and Wiegel[14] theorized that if the benefits of larger LN size and number were equally important and the total volume of LNs scales linearly with body mass, then LN size and number should scale with the square root of body mass ($M^{\frac{1}{2}}$). For comparison, we show that the spleen, like most organs, scales approximately linearly with body mass in Fig. 2A.

We relate the speed of antigen detection in the LN to theoretically predicted and empirically observed volume scaling observations with the formula, $M^{v-(t+d)}$, where M is mass, and v, t, and d are the scaling exponents relating LN volume, the number of T cells, and the number of DCs, respectively, to M. We define Initial First Contact Time (IFCT) as the time it takes for the very first naïve T cell to come into contact with a cognate antigen in a LN, and show that when larger LN have more T cells and DCs, IFCT is faster.

The benefit of more LNs is clear because a higher density of LNs reduces the average distance between potential infection sites and the closest LN and therefore the antigen transport time (Fig. 1, step 2)[15]. However, the benefit of larger LNs was previously not obvious, especially since Perelson and Wiegel[14] predict that *typical* search times should be independent of the LN volume. That is, if the density of cells is constant, then a typical T cell or B cell would find a fixed target in the same amount of time, for any LN volume.

However, if there were no benefit to larger LN volumes, it would be optimal to simply have as many LNs as possible to minimize the time for DCs to transport antigen to the LN (Fig. 1, step 2). Empirical data show that both the number and size of LNs increase with body mass, but sublinearly with exponents close to 1/2, but with the volume exponent slightly higher than the number exponent. One explanation for this was proposed in[14]: larger, and generally longer-lived mammals encounter a greater diversity of pathogens, and therefore need larger LNs to maintain a greater diversity of immune cells. Equation (4) suggests a complementary advantage to larger LNs: larger LNs hold more copies of T cells cognate to particular antigens, resulting in faster IFCT.

In previously published work[17], we present a mathematical model that predicts IFCT between searchers and targets distributed at random in a volume. We explored how the number of searchers, the distribution of searchers and targets, and the initial distances between searchers and targets affect IFCT. Here, we build on those models to make a mathematical prediction for IFCT scaling in LNs and test it in simulations. We show that the time to first T cell contact with a DC is invariant with body mass given a constant number of DC, as long as T cell density within LNs is fixed. Further, IFCT decreases when both T cell and DC density are constant. One key assumption is that there is a constant density of T cells in LNs (and this holds for any scaling of LN volume with M), so larger LNs contain more T cells in absolute terms. Thus, in larger LNs, the probability of a T cell–DC pair encountering each other increases, reducing expected times to initiate the adaptive immune response.

We base our analysis on the following simplifying Assumptions:

1. T cell density is constant; it does not vary systematically with LN volume or animal mass.

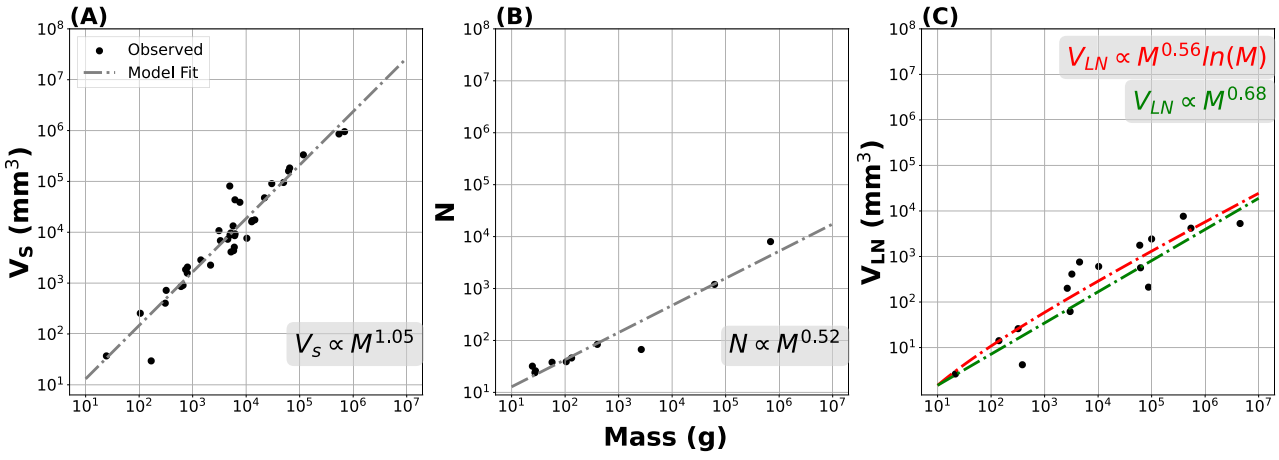

Fig. 2. Lymphoid organ scaling with mass. Each data point represents a species. Both axes are on a log scale. The dashed lines show the reported regression fits. **(A)** Spleen volume of 38 species is best fit by the regression cM^{μ} with $c = 1.2$ and exponent $\hat{\mu} = 1.05$ (95% CI [0.95, 1.2]). **(B)** Number of lymph nodes for 10 species is best fit by cM^{μ} with $c = 4$ and $\hat{\mu} = 0.52$ (95% CI[0.40, 0.64]). **(C)** Lymph node volume for 16 species is equally well fit in two ways: (1) a theoretically motivated fit including a logarithmic term $c_1 M^{\mu} \ln(c_2 M)$ (red line) with $c_1 = 1$, $c_2 = 1$, and $\hat{\mu} = 0.56$ (95% CI [0.18, 0.94]) and by (2) by a simpler scaling fit, $c_1 M^{\mu}$ (green line) with $c_1 = 1$, and $\hat{\mu} = 0.68$ (95% CI [0.51, 0.85]). The p-value of the exponents is significant at the 0.01 level.

2. T cells and DCs are uniformly distributed within the T cell zones of LNs.
3. Cell-cell encounters follow a memoryless exponential waiting-time distribution.
4. T cells move by unbiased diffusion in the LN.
5. Scaling exponents are not sensitive to prefactors that might represent details of particular subtypes of immune cells or pathogens, movement patterns of T cells, geometrical shapes of LNs or how cells enter LNs, nor to the noise inherent in data collected from published literature. We simplify the complex immune response in favor of a more general model.
6. We assume the density of DCs in LN can vary. We consider two bounding cases: a) the number of DCs is constant or b) the density of DCs is constant with respect to LN volume.
7. We do not know what fraction of naïve T cells are cognate to antigens produced from any particular pathogen. We model two alternative assumptions: a) the density of *cognate* T cells remains constant across LNs (proportional to the density of all T cells), or b) increased diversity of T cells dilutes the density of cognate T cells by a logarithmic factor.

Numerous agent-based and ODE models have explored how T cells scan antigen-bearing DCs, examining effects of motility, affinity, and spatial organization[18–30]. These studies demonstrate that individual T cell–DC contacts can be prolonged and that not every T cell must engage in order to initiate immunity. However, none has treated the *very first* cognate encounter (which we call IFCT) as a biologically meaningful threshold marking the true onset of the adaptive cascade.

IFCT marks the moment when a single cognate T cell first encounters its antigen-presenting DC. Any delay directly postpones the immune peak because this time determines the earliest possible start of exponential clonal expansion. Hence, IFCT sets a lower bound on how fast the peak can be reached. Unlike peak response timing, IFCT depends solely on search dynamics within LNs, making it a key measure for understanding how the sizes and numbers of LNs can compensate for slower physiology to preserve rapid detection.

Here, we show, both analytically and in agent-based simulations, that IFCT depends on the number of T cells and DCs involved in the search, and given more searchers in larger LNs, IFCT is equally fast or faster in larger mammals.

Time to initiate the adaptive immune response is the same in humans and mice

We first establish that the timing of the first detectable adaptive immune response is similar in humans and mice. Data on the timing of immune response are available for multiple pathogens in mice and humans because mice are the predominant model organism in immunological research, and human data are of direct clinical relevance. Table 1 shows that for a range of viral and bacterial pathogens, newly activated T cells are first detected in LNs or tissues in both species within 4–10 days, with a typical detection time of 6 days, following the activation of naïve T cells that had not previously encountered these antigens. The time to detect activated T cells reflects the time for cells to move, activate, and proliferate (Fig. 1, steps 1–6 if T cells are detected in LN, or steps 1–7 if detected in infected tissues). In the rest of this paper, we focus primarily on a subset of these steps, T cell search for cognate antigen-presenting DCs in LNs (Fig. 1, steps 3–5).

We note that the first detection of activated T cell populations is distinct from the peak T cell concentrations that are often measured in blood. It can take additional time to reach the peak after initial activation, particularly in larger animals. For example, peak T cell concentrations are observed in 5–10 days in mice[31,32] and 14–28 days in macaques and humans[33,34].

Quantitative measures of initial antigen-specific naïve T cell activation are scarce outside of mice and humans due to experimental and ethical constraints. While other species, such as swine, non-human primates, and certain rodents, are widely used in infectious-disease studies, detailed early adaptive response kinetics are rarely reported; many studies do not collect data before day 7 or day 10 post infection. While we did not find relevant reports of multiple different infections for species other than humans and mice, we did find the initial detection of T cells in macaques for SARS-CoV-2 and pigs for influenza were 7–10 days[56] and 6 days[57,58] respectively. These times are consistent with the data in Table 1. The consistency of times in Table 1 motivates the question - why is the timing of the initial immune response so similar across animals that are so different in size?

Empirical scaling of spleen size

Figure 2(A) shows that spleen volume[59,60] scales approximately linearly with mass (also see Table S1). A linear regression on log-log transformed data was used to derive an exponent, $\hat{\mu}$ of 1.05 with 95% CI [0.95, 1.2] and with $R^2 = 0.91$. The data are consistent with the expectation of linear scaling of spleen size with M. The data are also consistent with an additional logarithmic increase ($\ln(cM)$) (See Section S1.2). Such a nonlinear scaling could accommodate the predicted logarithmic increase in lymphocyte diversity with M hypothesized in[14].

Empirical scaling of lymph node number and size

Lymph node numbers and volumes were estimated from healthy adult animals using standardized geometric approximations; details of data selection, geometric assumptions, and measurement methodologies are provided in Supplementary Section S1.1. While there is substantial heterogeneity in LN volumes within each species (for example, human LNs range in diameter from $2\ \mathrm{mm}$ to $38\ \mathrm{mm}$), that variation is dominated by more than thousand-fold differences in LN volumes between the largest and smallest mammals in Supplementary Table S1. The scaling exponents we find by comparing across all species are consistent with the estimates we find comparing just between mice and humans, which are the best characterized species.

Wiegel and Perelson[14] propose LN number and size scaling based on two key assumptions: first, maximizing LN volume and number are equally important, and second, the total LN volume scales approximately linearly,

proportional to body mass M (noting that scaling is also predicted to accommodate a logarithmic increase in T cell diversity with M). Based on these assumptions, they predict that the volume of a typical LN, V_{LN}, scales as follows, where c is a constant,

$$V_{\mathrm{LN}} \propto M^{\frac{1}{2}} \ln(cM). \tag{1}$$

The number of LNs, N_{LN}, scale as,

$$N_{\mathrm{LN}} \propto M^{\frac{1}{2}}. \tag{2}$$

Figure 2(B) shows the scaling of LN number. The best fit for 10 species, with M ranging from 24 g mice to 690 kg horses, for $N_{LN} = cM^{\mu}$ is $c = 3.8, \hat{\mu} = 0.52$, 95% CI [0.40, 0.64], consistent with the Perelson-Wiegel prediction of $\frac{1}{2}$ exponent with $R^2 = 0.93$.

Figure 2(C) shows the scaling of LN volume with mammal mass for 16 species from 24 g mice to 4500 kg elephants. Regression of the form $V_{LN} = c_1 M^{\mu} \ln(c_2 M)$, produces, $c_1 = 1$, and $c_2 = 1$, $\hat{\mu} = 0.56$ (95% CI [0.18, 0.94]) with $R^2 = 0.84$. While this is consistent with the predicted $\frac{1}{2}$ exponent, the inclusion of the log term allows flexibility in the fit, accommodating a very wide range of scaling exponents. Excluding the logarithmic term yields a higher exponent of $\hat{\mu} = 0.68$ (95% CI [0.51, 0.86]) (Fig. 2C), with R^2 = 0.83. The Akaike's Information Criterion values for the models with and without logarithmic terms are very similar, −23.42 and −23.26, respectively (See Section S1.3 for computation).

Interestingly, both scaling relationships suggest that total LN volume (the number of LN multiplied by typical LN volume) scales superlinearly with body mass, as either $M^{1.08} ln(M)$ or $M^{1.20}$. Despite sublinear scaling of both LN number and size, the total volume of LNs increases slightly superlinearly with body mass, implying that larger animals allocate a slightly larger fraction of their body volume to lymphoid tissue.

Since the data roughly align with the theoretical predictions given in Equations (1) and (2), as well as the linear scaling of spleen volume, we can estimate human LN volume, LN number, and spleen volume relative to those of mice. The theoretical expectation is that LN volume 350 times larger, LN number 50 times larger, and spleen 2,500 times larger in humans. Actual values from Table S1 are within a factor of two of these approximations. Given the more than three orders of magnitude difference in the sizes of humans and mice, predictions that are within a factor of two of empirical estimates are useful approximations, similar to the physiological scaling predictions of heart rates, breathing rates, and gestation times described in the introduction. Given the similar fit for a simpler powerlaw equation $V_{LN} \propto M^{\frac{2}{3}}$, we include this scaling as well as the theoretically predicted $M^{\frac{1}{2}} ln(M)$ scaling.

Predicting initial first contact times

We derive a prediction for the time for the first T cell to find its cognate antigen-presenting DC within a LN, and then validate the prediction with our agent-based model (See Section S1.6 for detailed understanding of our agent-based model). We first consider a generic search problem between a population of T cell searchers (N_{TC}) and a population of targets DCs (N_{DC}) in a LN volume (V_{LN}). In Section S1.4, we derive an equation, Derivation 1, for IFCT, represented by the variable τ_{init}:

$$\tau_{\mathrm{init}} \propto \frac{\lambda}{N_{\mathrm{TC}} N_{\mathrm{DC}}} \tag{3}$$

where $\lambda$is defined as the mean first-contact time in a volume between a single T cell and a single DC. Celli et. al[23]. showed that λ scales linearly with volume ($\lambda \propto V_{LN}$) if the searcher and target are randomly placed and the searcher moves using Brownian motion (Definition 1 in the Supplement). Since we have the product of N_{TC} and N_{DC} in the denominator, search times decrease linearly with increases in both T cells and DCs.

Scaling of Initial First Contact Time (τ_{init}): Assuming diffusive motion of cells within the LN, let LN volume scale as $V_{LN} \propto M^{v}$, the number of cognate T cells as $N_{\mathrm{TC}} \propto M^{t}$, and the number of cognate DCs as $N_{\mathrm{DC}} \propto M^{d}$. Then IFCT scales as:

$$\tau_{\mathrm{init}} \propto \frac{V_{LN}}{N_{\mathrm{TC}} N_{\mathrm{DC}}} \propto \frac{M^{v}}{M^{t} M^{d}} = M^{v-(t+d)} \tag{4}$$

Equation (4), allows us to explore how different assumptions about how the mass scaling of LN volumes, T cell numbers and DC numbers affect the time to initiate an immune response. Equation (4) yields three scaling regimes:

- Case *i*: If $v < (t + d)$, then τ_{init} decreases with M. This represents faster scaling of τ_{init} in larger animals in *systemic infections*. This occurs under Assumption 6a where $d = v$.
- Case *ii*: If $v = (t + d)$, then τ_{init} is invariant with M (constant τ_{init}). This represents constant numbers of DCs with respect to M in *localised infections* when $t = v$ and $d = 0$. This occurs under Assumption 6b with Assumption 7a.
- Case *iii*: If $v > (t + d)$, then τ_{init} increases with M. This occurs with Assumptions 6b with Assumption 7b where $d = 0$ and $t < v$ by a logarithmic factor.

We start with Assumption 7a that the density of cognate T cells are constant within LNs. In that case, it is the density of DCs that determine whether the scaling regime for τ_{init} is Case *i* or *ii*. Following Assumption 6a or

6b, we consider two regimes as assumed bounds on what is biologically realistic. To analyze the systemic Case *i*, we assume the density of DCs carrying antigen in the LN is constant ($d = v = t$, Assumption 6a). A constant density of DC's could be expected for a systemic infection, for example SARS-CoV-2 that infects some fraction of the lung, producing more total amounts of antigen, proportional to lung mass and body mass, *M*.

In this case, cognate T cell and DC counts scale linearly with LN volume, i.e., both are constant density, so $t = d = v$. Thus, $\tau_{\text{init}} \propto M^{-v}$, and first contacts are faster in bigger animals. How much faster depends on the scaling exponent *v*.

In Fig. 3A, we simulate LN volumes that scale according to Wiegel and Perelson's theory (Assumption 7b), where $v = 1/2$, that is, LN size increases by a factor of $M^{1/2}$ multiplied by ln(*M*) to accommodate increased T cell repertoire diversity in larger animals. Thus, the density of particular T cells cognate to the antigens in the current infection increases by $M^{1/2}$ but decreases by ln(*M*) (See Table S4). Figure 3A validates that the simulated τ_{init} is consistent with the predicted scaling, $M^{-1/2}ln(M)$. τ_{init} still decreases, but modified by a log factor generating a curvilinear fit (red line). Note that simulated volumes appear at the top of each panel and the corresponding animal mass is indicated by the x-axis of Fig. 3.

In the second case (Assumption 6b and Case *ii*) a localized infection might produce a fixed amount of infection, leading to a *constant number* of antigen-bearing DCs in the LN, so that the density of DC's decline with LN volume. For $V_{LN} \propto M^{0.5} \ln(cM)$ we predict that τ_{init} is constant, as is validated in simulations in Fig. 3B. The result produces a curvilinear logarithmic increase in τ_{init}, following Assumption 6b, 7b and Case *iii* (red line).

Median first contact times

In order to compare τ_{init} with the previous models that considered the typical time for an average T cell to contact its cognate DC, we also model the median first-contact times ($\bar{\tau}$), the time for a typical T cell to contact its cognate antigen-bearing DC.

We model this for both systemic and local infection under Assumption 7b, following the approach outlined in[14]. According to Perelson and Wiegel in[14], $\bar{\tau}$ doesn't depend on the number of T cells (Derivation 4 in Supplementary Material). We calculated ($\bar{\tau}$) from the same simulations as (τ_{init}), but running until all T cells had their first contact with a DC and then calculating the median of those times. Table 2 shows the predicted values of $\bar{\tau}$ for both systemic and localized infections. Figure 3 shows how both predicted and simulated $\bar{\tau}$ scale for systemic (Panel A) and localized (Panel B) infections (blue lines). See Section S1.4 for full derivation of τ_{init} and $\bar{\tau}$ for different cases and Table S2 for all the notations used in this work.

For systemic infections, assuming the theoretical model ($\tau_{init} \propto M^{-\frac{1}{2}} \ln(cM)$), then $\bar{\tau}$ scales logarithmically with body mass as $M^0 \ln(cM)$ (See Supplement Prediction 4.1); for the local infection, where

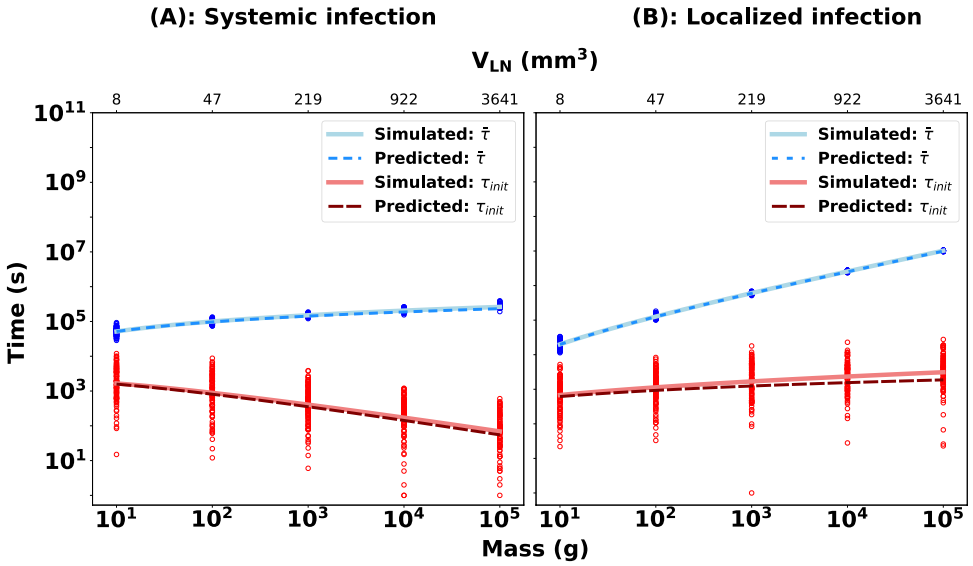

Fig. 3. Theoretical Predictions vs. Agent-Based Simulations for Initial First Contact Time (τ_{init}) and Median First Contact Time ($\bar{\tau}$) in Lymph Nodes. Simulation data (circles) are compared to predictions (dashed) and best-fit curves (solid) under two infections: Panel **(A)** For systemic infection ($N_{DC} \propto M^{\frac{1}{2}}$), predicted $\tau_{init} \propto M^{-1/2} \ln(cM)$ (dashed red), fitted $\hat{\mu} = -0.48 \pm 0.10$ (solid red). The predicted median first-contact time is $\bar{\tau} \propto M^{\mu} \ln(cM)$ with, $\mu = 0$ (dashed blue line). The best fit (solid blue line) for the corresponding simulated data (blue points) gives the exponent $\hat{\mu} = 0.17 \pm 0.010$. **(B)** Localized infection ($N_{DC} \propto M^0$): predicted $\tau_{init} \propto M^0 \ln(cM)$ (dashed red), fitted $\hat{\mu} = 0.040 \pm 0.100$ (solid red). The predicted median first-contact time, is $\bar{\tau} \propto M^{\mu} \ln(cM)$ with $\mu = 0.5$ (dashed blue line). The best fit (solid blue line) to the simulated data (blue points) gives the value for the exponent, $\hat{\mu} = 0.50 \pm 0.010$. The simulations for both cases are consistent with theoretical predictions. Each circle represents the simulation result of 30 simulation replicates for $\bar{\tau}$ and 100 replicates for τ_{init} at each estimated LN volume.

Mass	Initial First Contact Time				Median First Contact Time			
	$N_{DC} \propto M^{\frac{1}{2}}$		$N_{DC} = \text{Constant}$		$N_{DC} \propto M^{\frac{1}{2}}$		$N_{DC} = \text{Constant}$	
	Brownian Motion	Persistent Random Walk	Brownian Motion	Persistent Random Walk	Brownian Motion	Persistent Random Walk	Brownian Motion	Persistent Random Walk
24 g (Mouse)	22 min	28 min	14 min	14 min	1 d	0.80 d	0.65 d	0.49 d
1 kg	6.8 min	9.1 min	28 min	28 min	2.3 d	1.7 d	9.1 d	7 d
62 kg (Human)	1.4 min	1.6 min	49 min	60 min	3.6 d	2.9 d	120 d	89 d

Table 2. DC-T cell ***Initial*** and ***Mean*** first contact times. We consider 2 cases: i) assuming the number of DC in LN scales with $M^{0.5}$ (constant density of antigen-bearing DC from a systemic infection) and ii) a constant number of DC in LN ($N_{DC} = \text{Constant}$). We estimate times for each case, considering that T cells move in using either *Brownian motion or a persistent random walk*.

$\tau_{init} \propto M^0 \ln(cM)$, then $\bar{\tau}$ scales as $M^{\frac{1}{2}} \ln(cM)$ (See Supplement Prediction 4.2). In both cases, τ_{init} is a factor of M^v faster than $\bar{\tau}$. τ_{init} takes less than one hour in humans and mice, but for systemic infection $\bar{\tau}$ takes 1 day for a mouse and over 3 days for a human (see Table 2). For localized infections, $\bar{\tau}$ also takes about 1 day for a mouse but takes 100 days for a human! In this case, the typical T cell contact ($\bar{\tau}$) happens long after the first T cells have begun to activate and exponentially replicate. In some cases, the typical T cell would not even activate until long after the infection is resolved. $\bar{\tau}$ is 65 times slower than τ_{init} for a mouse, but 3700 times slower for a human. These calculations emphasize the critical role of timely first encounters in initiating an effective immune response, particularly in larger animals. We argue that τ_{init} is more consequential than $\bar{\tau}$ for the clonal expansion of effector T cells that exponentially replicate (Fig. 1, step 6) after activation and then travel to tissues to fight pathogens (Fig. 1, step 7), although $\bar{\tau}$ may be an important factor in determining the magnitude or timing of the peak T cell response.

The faster τ_{init} for systemic infections, and approximately invariant τ_{init} for localised infections in Fig. 3 arise because the time for the rare fortunate *first* contact is expedited when more T cells are present. However, the advantage of a large population doesn't benefit the *typical* T cell. Additionally, the last T cell-DC encounter takes far longer when there are more T cells. We fit the empirical data to two predictions: 1) the theoretical prediction ($V_{LN} \propto M^{1/2} ln(M)$) and 2) the more parsimonious ($V_{LN} \propto M^{2/3}$) prediction to identify a better fit to the data, shown in Fig. 2. We use $V_{LN} \propto M^{2/3}$, as a simple approximation of the empirical data.

To further test our model, we reanalyze the empirical data presented in[61] using the IFCT model (see Section S2 for details). The model in[61], assumes that contact between all T cells and DCs happens at a time corresponding to $\bar{\tau}$. We implement this assumption in a Median model (see Section S2 for details) using the median contact time from our simulations. In Fig. S2, we compare T cell population dynamics from our IFCT model, which accounts for the time for each individual T cell to first contact its DC target, with data from[61] over time and with data from the Median model. We parameterize our systemic infection model to reflect epitope-specific T-cell clone immunodominance and precursor frequency by using empirical activation times; NP118 and GP283 are LCMV-derived epitopes presented via MHC class I. NP118 is immunodominant, with a shorter estimated time to activation (~6.8 hours). GP283 is subdominant, with a longer estimated activation time (18.8 hours). After 5–6 days post-infection, the Median model predicts peak T cell populations of 3.9×10^7 for NP118 and 1.2×10^6 for GP283, whereas the IFCT model predicts more than double these values at 9.1×10^7 and 3.4×10^6. Thus, in a mouse, a model using IFCT would predict more than twice the peak number of T cells compared to a Median model (See Table S6).

We then scale the models up to estimate the peak T cell population in a larger volume. Compared to the Median model, the IFCT model predicts peak T cell populations that are 40-times larger for the larger LNs (Fig. S3). Thus, by accounting for the rare early first contact, we estimate far larger peak T cell populations, particularly in larger animals. Thus, not only is search faster in bigger LNs, but also, earlier contacts make many more T cells during the exponential growth phase.

We predict and simulate the corresponding τ_{init} shown in Fig. S1 (see Section S1.6). We find the theoretical model convincing because it accounts for increases in T cell diversity. However, it is not clear whether increased T cell diversity results in a logarithmic dilution in the density of cognate T cells (because there are more *other* T cells that are not cognate to the antigens of a particular infection). Alternatively, the increased diversity may result in more clonal lines of T cells that are cognate to more antigens (potentially counteracting the dilution). Without data to distinguish between these alternatives, we use the theoretical model (with logarithmic reductions in density of cognate T cells) and the simple scaling model (where cognate T cell density is constant) to cover both of these cases. Table S3 shows that these different assumptions make little practical difference. Importantly, τ_{init} is nearly as fast or faster in bigger LN, and τ_{init} is much faster than $\bar{\tau}$, by a factor of M^v in all of our modeled scenarios.

Discussion

The time to initiate the adaptive immune response is similar in mice and humans despite three-orders of magnitude difference in their mass. This unusual mass invariance in initial adaptive immune response times is accompanied by an unusual scaling of the organs in which adaptive immunity is initiated. LN number and volume both scale sublinearly with mammal mass (M), and the total volume of LNs scales slightly superlinearly

with mass. The data are insufficient to differentiate whether total LN volume increases proportional to $M^1 \ln(M)$ following Perelson and Wiegel's earlier theoretical predictions, or with a simpler $M^{1.2}$ scaling equation.

Theory[14] predicts one-half exponents for the number and average volume of LN if scaling up LN size and LN number have equal benefits and the total LN volume is constrained to scale approximately linearly with animal mass. The empirical data are roughly consistent with this theoretical prediction. An obvious benefit of having more LNs as animal mass increases is that the distance from a site of infection to the nearest LNs is reduced, reducing time to transport antigens to the LNs[14,15]. The analysis above shows a previously undescribed benefit of larger LNs: the search for antigen-bearing DCs happens in equal time or faster in larger LNs as long as T cell density is constant. Given that LN are larger in larger mammals, T cells initiate adaptive immunity by contacting DCs in LNs nearly as fast or faster in larger animals.

The logic is simple: if larger LNs contain more T cells and more DCs in absolute terms, then the first "lucky" T cell that quickly contacts a DC will be faster. This speed up is not because T cells and DCs are closer *on average*, but because very short distances to cognate DCs and very fortuitous movements toward DCs become more likely given larger populations. Since immune activation can be initiated by fortuitous early interactions, this enrichment in the tail of the spatial distance distribution dramatically reduces τ_{init}. Thus, the first time any T cell contacts its cognate DC in a LN can occur in minutes, compared to days for the first time a typical T cell contacts its cognate DC ($\bar{\tau}$).

Our IFCT model, parameterized to match empirical observations of T cell population growth in mouse spleens, shows a two-fold increase in T cell population compared to a model that only considers $\bar{\tau}$ rather than τ_{init} (Section S2). When scaled to a larger spleen or LN (i.e., the spleen of a macaque or the LN of a cow) the peak number of T cells grows 40-fold larger when exponential growth is modeled to start at τ_{init} rather than $\bar{\tau}$. By accounting for exponential growth intiated by the earliest T cells to contact cognate antigen-bearing DCs, growth of T cell populations could fight pathogens more effectively than was previously modeled.

Distributed Lymphatic versus Centralized Cardiovascular Networks: According to metabolic scaling theory, quarter-power scaling relationships[2,3] arise from systematic increases in transport time in larger animals, based on the assumption that resources flow outwards from a single, central source (the heart) through a fractal circulatory network. In contrast, the immune system relies on a distributed architecture of LNs[62], each acting as an independent hub where naïve lymphocytes and antigen-bearing DCs meet. Not only does this decentralization permit multiple, parallel activation sites, but individual nodes can also recruit immune cells from distant regions via the lymphatic and blood vessels during an active infection. This alternative mode of resource distribution underpins our key finding: Bigger LNs enable faster initial T-cell–DC contacts as body mass increases. This is because the absolute numbers of both T cells and DCs in each LN grow with LN volume, speeding up τ_{init}. This distributed architecture with more LN in larger animals means LN are, on average, closer to sites of infection than they would be in a centralized model. This reduces transport times to LN. They are also bigger, reducing search times within LN. Empirically, this allows the adaptive immune response to be initiated in constant time (Table 1) across animals that vary substantially in body size. This meets the evolutionary imperative to detect and control exponentially replicating pathogens in large as well as small mammals.

Here, we have highlighted one advantage that the distributed lymphatic network provides: balancing the speed of transport to LNs that comes with many small LNs with the faster detection of antigen within a few large LNs. However, there are other constraints on LN size and number. For example, LN must be big enough to hold a sufficient diversity of B and T cells and a sufficient number of exponentially growing activated B and T cells during an infection; both of these also vary with animal size.

Caveats, Limitations and Open Questions: While our modeling framework provides mechanistic insights into how LN sizes and numbers enable rapid initial T cell–DC contacts across body sizes, readers are referred to Supplementary Section S3 for a detailed discussion of underlying assumptions, empirical uncertainties, as well as limitations and potential extensions of our approach. A particularly noteworthy caveat is that some values in our datasets are difficult to measure precisely. The number of LNs in an animal may be under-counted, and average LN size may be overestimated if the smallest LN are missed and these factors may particularly skew estimates in larger species. Additionally the structure of LN can vary across species.

We have simplified complex immunology and anatomy in favor of a simpler model. The size of the T cell zone relative to the measured LN volume, the effective T cell–DC encounter radius, the shape of LN and the diffusion coefficient of T cells could all affect our IFCT models. Further, there is variation among the myriad subtypes of immune cells, receptors and molecules. However, we assume there is not substantial systematic variation across body sizes, so that they do not change how search times scale with mass. While we intend our analysis to be general enough to apply to both LN and spleens, the processes of transporting antigens to these tissues and the architecture of these tissues are different, so the absolute timing of first contacts may be different in spleens and LNs.

It remains an open question to fully explain how the scaling of LN size and number, the complex dynamics of replicating T cells[63], and the movement of both antigens and T cells into LN[62] result in such similar times (6 days) that the first antigen-specific replicated T cells are observed in both mice and humans in Table 1. Such an explanation requires not just analysis of search times within LNs (Figure 1, steps 3 –5), but also times for DC to ingest and carry antigen to LN (steps 1 and 2), and subsequently for T cells to replicate, differentiate and travel back to infected tissue (steps 5–7).

Despite these caveats, several observations support our estimated scaling exponents and conclusions. The LN size and number scalings from the best studied species, mice and humans, are consistent with the $N_{LN} \propto M^{1/2}$ and the two formulations we consider for LN volume: $V_{LN} \propto M^{1/2} ln(M)$ and $V_{LN} \propto M^{2/3}$ (see Supplemental Section S1). We also tested model sensitivity to alternative non-Brownian movement patterns of T cells[29] and found that empirically observed persistent motion decreases cell contact times by a relatively small factor (see Table S5), but does not alter the scaling exponent, consistent with Assumption 5.

Our models are also consistent with the timing of empirical T cell dynamics in Supplemental Section S2. Finally, our main conclusions hold regardless of scaling exponents: τ_{init} is similar across body sizes for localized infections, faster in larger animals for systemic infections, and substantially faster than $\bar{\tau}$ for all infections.

Broader Implications: Our analysis shows a benefit of large size that has not been previously appreciated. While bigger animals are usually slower, here we show that τ_{init} is faster in larger mammals. This makes sense intuitively because when there are more searchers (or targets[64]), the first target is found faster. This phenomenon has been studied by physicists as extreme first passage times[65]. In contrast to our findings of a linear speedup with size, previous extreme first passage time (EFPT) analyses find a much slower speedup that is only logarithmic with the number of searchers. The differences arise because EFPT considers an infinite number of searchers, all starting their search at the same physical location, with search trajectories that overlap. In contrast, in the LN search problem, a finite number of dispersed searchers in the 3D volume of a LN can be considered independent of each other, leading to the much greater (linear) advantage of large search populations that we identify here.

The different scaling properties of IFCT and typical first contact times are particularly relevant when the first contact causes a cascade of downstream events. In the initiation of adaptive immunity, when cognate T cells contact DCs, the T cells replicate (Fig. 1, step 5), and changes occur in the LN, including slowing the egress of other T cells. Thus, the first contact changes the dynamics of subsequent searches. Further, the exponential growth of T cells begins once the first contact is made. Subsequent T cell contacts can amplify the T cell response, but τ_{init} causes the first T cell replication that produces activated T cells to migrate to fight infection in tissues (Fig. 1, step 7). The first arrival time of T cells in tissue is important in controlling exponentially growing pathogens, as has been shown in response to SARS-CoV-2 infection[34] and in our simulations of the timing of T cell response[30].

Understanding the different scaling properties of initial versus typical first contact times is also relevant for other immunological processes, for example, the B cell search for T cells in LN (modeled in[14]) and effector T cell search for infected cells in peripheral tissue (modeled in[30]). The analysis here suggests that initial contacts may happen faster in larger animals with more immune cells, but last contacts might take longer[66]. Last contacts may be relevant for understanding the dynamics of final clearance of infections.

This variation in immune response can affect the timing and duration of infection and infectiousness in animals of different sizes; this, in turn, can affect how diseases spread across animal communities[67]. The distinct scaling properties of first, typical, and last search times warrant further study in immunology and biology more broadly. The different times to achieve typical, first, and last search events affect any biological search that involves large numbers of searchers. For example, the first ant in a colony that finds food should similarly depend on colony size, and when that first event happens, communication of the food location changes the search times for the typical ant in the population[68,69]. Similarly, the first individual with a rare genetic mutation that confers some fitness advantage occurs faster in larger populations and then changes the downstream dynamics. Thus, we suggest that understanding how the timing of the initial first successful search depends on the number of searchers is an essential and previously neglected question in immunology and, more generally, in biology.

Data availability

All data for spleen volume, LN volume, and LN number used in this paper are collected from the published literature and included in a Supplementary in Table S1. Raw data files for initial and median first contact time generated from our model are available online at Dryad: https://doi.org/10.5061/dryad.5x69p8df1 All figures, except for Fig. 1, are generated using Python 3 in a Jupyter Notebook and Adobe Illustrator. Figure 1 was generated using BioRENDER. The code for our agent-based model, mathematical analysis, and figure generation is available at https://github.com/BCLab-UNM/BiggerIsFaster.

Received: 18 March 2025; Accepted: 11 November 2025
Published online: 29 December 2025

References

1. Kleiber, M. Body size and metabolic rate. *Physiological reviews* **27**(4), 511–541 (1947).
2. West, G. B., Brown, J. H. & Enquist, B. J. A general model for the origin of allometric scaling laws in biology. *Science* **276**(5309), 122–126 (1997).
3. Banavar, J. R. et al. A general basis for quarter-power scaling in animals. *Proceedings of the National Academy of Sciences* **107**(36), 15816–15820 (2010).
4. Calder, W. A. *Size, function, and life history* (Harvard University Press, 1984).
5. Lindstedt, S. & Calder, W. III. Body size, physiological time, and longevity of homeothermic animals. *The Quarterly Review of Biology* **56**(1), 1–16 (1981).
6. Mordenti, J. Man versus beast: pharmacokinetic scaling in mammals. *Journal of pharmaceutical sciences* **75**(11), 1028–1040 (1986).
7. Charnov, E. L., Warne, R. & Moses, M. Lifetime reproductive effort. *The American Naturalist* **170**(6), E129–E142 (2007).
8. West, S. S. G. B. et al. *Scaling in biology* (Oxford University Press on Demand, 2000).
9. Peters, R. H. & Peters, R. H. *The ecological implications of body size* Vol. 2 (Cambridge University Press, 1986).
10. Savage, V. M. et al. The predominance of quarter-power scaling in biology. *Functional Ecology* **18**(2), 257–282 (2004).
11. Clarke, J., Shelton, J., Venning, G., Hamer, J. & Taylor, S. The rhythm of the normal human heart. *The Lancet* **308**(7984), 508–512 (1976).
12. Meijer, M., Spruijt, B., Van Zutphen, L. & Baumans, V. Effect of restraint and injection methods on heart rate and body temperature in mice. *Laboratory animals* **40**(4), 382–391 (2006).
13. Perelson, A.S., Bragg, J.G., Wiegel, F.W.: The complexity of the immune system: scaling laws. *Complex systems science in biomedicine*. 451–459 (2006).
14. Perelson, A. S. & Wiegel, F. W. Scaling aspects of lymphocyte trafficking. *Journal of theoretical biology* **257**(1), 9–16 (2009).
15. Banerjee, S. & Moses, M. Scale invariance of immune system response rates and times: perspectives on immune system architecture and implications for artificial immune systems. *Swarm Intelligence* **4**(4), 301–318 (2010).
16. Althaus, C.L.: Of mice, macaques and men: scaling of virus dynamics and immune responses (2015).

17. Ferdous, J., Matthew Fricke, G., Moses, M.E.: More Is Faster: Why Population Size Matters in Biological Search. *Journal of Computational Biology* **31** (5), 429–444 (2024), pMID: 38754139, https://doi.org/10.1089/cmb.2023.0296, https://doi.org/10.1089/cmb.2023.0296.
18. Moreau, H. D., Bogle, G. & Bousso, P. A virtual lymph node model to dissect the requirements for T-cell activation by synapses and kinapses. *Immunology and cell biology* **94**(7), 680–688 (2016).
19. Bogle, G. & Dunbar, P. R. Agent-based simulation of T-cell activation and proliferation within a lymph node. *Immunology and cell biology* **88**(2), 172–179 (2010).
20. Bogle, G., Dunbar, P.R.: On-lattice simulation of T cell motility, chemotaxis, and trafficking in the lymph node paracortex (2012).
21. Riggs, T., et al.: A comparison of random vs. chemotaxis-driven contacts of T cells with dendritic cells during repertoire scanning. *Journal of theoretical biology* **250** (4), 732–751 (2008).
22. Gong, C.: *Quantifying the Generation of T Cell Immunity using a Systems Biology Approach.*, Ph.D. thesis (2015).
23. Celli, S. et al. How many dendritic cells are required to initiate a T-cell response?. *Blood, The Journal of the American Society of Hematology* **120**(19), 3945–3948 (2012).
24. Beltman, J. B., Marée, A. F. & De Boer, R. J. Analysing immune cell migration. *Nature Reviews Immunology* **9**(11), 789–798 (2009).
25. Graw, F. & Regoes, R. R. Investigating CTL mediated killing with a 3D cellular automaton. *PLoS computational biology* **5**(8), e1000466 (2009).
26. Donovan, G. M. & Lythe, G. T-cell movement on the reticular network. *Journal of theoretical biology* **295**, 59–67 (2012).
27. Regoes, R. R., Barber, D. L., Ahmed, R. & Antia, R. Estimation of the rate of killing by cytotoxic T lymphocytes in vivo. *Proceedings of the National Academy of Sciences* **104**(5), 1599–1603 (2007).
28. Textor, J. et al. Random migration and signal integration promote rapid and robust T cell recruitment. *PLoS computational biology* **10**(8), e1003752 (2014).
29. Fricke, G. M., Letendre, K. A., Moses, M. E. & Cannon, J. L. Persistence and adaptation in immunity: T cells balance the extent and thoroughness of search. *PLoS Computational Biology* **12**(3), e1004818 (2016).
30. Moses, M. E. et al. Spatially distributed infection increases viral load in a computational model of SARS-CoV-2 lung infection. *PLoS computational biology* **17**(12), e1009735 (2021).
31. Zhuang, Z., et al.: Mapping and role of T cell response in SARS-CoV-2–infected mice. *Journal of Experimental Medicine* **218** (4) (2021).
32. Miao, H. et al. Quantifying the early immune response and adaptive immune response kinetics in mice infected with influenza A virus. *Journal of virology* **84**(13), 6687–6698 (2010).
33. Mattoo, S.-u.-S., Myoung, J.: T cell responses to SARS-CoV-2 in humans and animals. *Journal of Microbiology.* 1–14 (2022).
34. Sette, A. & Crotty, S. Adaptive immunity to SARS-CoV-2 and COVID-19. *Cell* **184**(4), 861–880 (2021).
35. Owens, S. L., Osebold, J. & Zee, Y. Dynamics of B-lymphocytes in the lungs of mice exposed to aerosolized influenza virus. *Infection and immunity* **33**(1), 231–238 (1981).
36. Friberg, H. et al. Cross-reactivity and expansion of dengue-specific T cells during acute primary and secondary infections in humans. *Scientific reports* **1**(1), 1–9 (2011).
37. Keating, R. et al. Potential killers exposed: tracking endogenous influenza-specific CD8+ T cells. *Immunology and cell biology* **96**(10), 1104–1119 (2018).
38. Brown, T., Murphy, B., Radl, J., Haaijman, J. & Mestecky, J. Subclass distribution and molecular form of immunoglobulin A hemagglutinin antibodies in sera and nasal secretions after experimental secondary infection with influenza A virus in humans. *Journal of clinical microbiology* **22**(2), 259–264 (1985).
39. Tamura, S.-I. & Kurata, T. Defense mechanisms against influenza virus infection in the respiratory tract mucosa. *Jpn J Infect Dis* **57**(6), 236–47 (2004).
40. De Boer, R. J., Homann, D. & Perelson, A. S. Different dynamics of CD4+ and CD8+ T cell responses during and after acute lymphocytic choriomeningitis virus infection. *The Journal of Immunology* **171**(8), 3928–3935 (2003).
41. Brenner, G. J., Cohen, N. & Moynihan, J. A. Similar immune response to nonlethal infection with herpes simplex virus-1 in sensitive (BALB/c) and resistant (C57BL/6) strains of mice. *Cellular immunology* **157**(2), 510–524 (1994).
42. Coles, R. M., Mueller, S. N., Heath, W. R., Carbone, F. R. & Brooks, A. G. Progression of armed CTL from draining lymph node to spleen shortly after localized infection with herpes simplex virus 1. *The Journal of Immunology* **168**(2), 834–838 (2002).
43. Guvenel, A. et al. Epitope-specific airway-resident CD4+ T cell dynamics during experimental human RSV infection. *The Journal of clinical investigation* **130**(1), 523–538 (2020).
44. Homann, D., Teyton, L. & Oldstone, M. Differential regulation of antiviral T-cell immunity results in stable CD8+ but declining CD4+ T-cell memory. *Nature medicine* **7**(8), 913–919 (2001).
45. McAloon, C. et al. Incubation period of COVID-19: a rapid systematic review and meta-analysis of observational research. *BMJ open* **10**(8), e039652 (2020).
46. Koblischke, M., et al.: Dynamics of CD4 T cell and antibody responses in COVID-19 patients with different disease severity. *Frontiers in medicine* **7** (2020).
47. Jones, T.C., et al.: Estimating infectiousness throughout SARS-CoV-2 infection course. *Science* **373** (6551), eabi5273 (2021).
48. Rai, B., Shukla, A., Dwivedi, L.K.: Incubation period for COVID-19: a systematic review and meta-analysis. *Journal of Public Health*. 1–8 (2021).
49. Schulien, I. et al. Characterization of pre-existing and induced SARS-CoV-2-specific CD8+ T cells. *Nature medicine* **27**(1), 78–85 (2021).
50. Lei, Q., et al.: Antibody dynamics to SARS-CoV-2 in asymptomatic COVID-19 infections. *Allergy* (2020).
51. Iyer, A.S., et al.: Dynamics and significance of the antibody response to SARS-CoV-2 infection. *MedRxiv* (2020).
52. Schmaler, M., Jann, N. J., Ferracin, F. & Landmann, R. T and B cells are not required for clearing Staphylococcus aureus in systemic infection despite a strong TLR2-MyD88-dependent T cell activation. *The Journal of immunology* **186**(1), 443–452 (2011).
53. Brown, A. F. et al. Memory Th1 cells are protective in invasive Staphylococcus aureus infection. *PLoS pathogens* **11**(11), e1005226 (2015).
54. Khatib, R. et al. Time to positivity in Staphylococcus aureus bacteremia: possible correlation with the source and outcome of infection. *Clinical infectious diseases* **41**(5), 594–598 (2005).
55. Ridder, M. J. et al. Kinetic characterization of the immune response to methicillin-resistant Staphylococcus aureus subcutaneous skin infection. *Infection and Immunity* **90**(7), e00065-22 (2022).
56. Nelson, C.E., et al.: Mild SARS-CoV-2 infection in rhesus macaques is associated with viral control prior to antigen-specific T cell responses in tissues. *Science immunology* **7** (70), eabo0535 (2022).
57. Khatri, M. et al. Swine influenza H1N1 virus induces acute inflammatory immune responses in pig lungs: a potential animal model for human H1N1 influenza virus. *Journal of virology* **84**(21), 11210–11218 (2010).
58. Lange, E. et al. Pathogenesis and transmission of the novel swine-origin influenza virus A/H1N1 after experimental infection of pigs. *Journal of General Virology* **90**(9), 2119–2123 (2009).
59. Mebius, R. E. & Kraal, G. Structure and function of the spleen. *Nature reviews immunology* **5**(8), 606–616 (2005).
60. Lewis, S.M., Williams, A., Eisenbarth, S.C.: Structure and function of the immune system in the spleen. *Science immunology* **4** (33), eaau6085 (2019).
61. De Boer, R. J. et al. Recruitment times, proliferation, and apoptosis rates during the CD8+ T-cell response to lymphocytic choriomeningitis virus. *Journal of virology* **75**(22), 10663–10669 (2001).

62. Ferdous, J., Fricke, G.M., Moses, M.E.: Modeling Immune Search Through the Lymphatic Network, in *International Conference on Swarm Intelligence*, 332–340 (Springer, 2022).
63. De Boer, R. J. & Perelson, A. S. Quantifying T lymphocyte turnover. *Journal of theoretical biology* **327**, 45–87 (2013).
64. Delgado, M. I., Ward, M. J. & Coombs, D. Conditional mean first passage times to small traps in a 3-D domain with a sticky boundary: applications to T cell searching behavior in lymph nodes. *Multiscale Modeling & Simulation* **13**(4), 1224–1258 (2015).
65. Lawley, S. D. Universal formula for extreme first passage statistics of diffusion. *Physical Review E* **101**(1), 012413 (2020).
66. Lawley, S. D. & Johnson, J. Slowest first passage times, redundancy, and menopause timing. *Journal of Mathematical Biology* **86**(6), 90 (2023).
67. Downs, C. J., Schoenle, L. A., Han, B. A., Harrison, J. F. & Martin, L. B. Scaling of host competence. *Trends in parasitology* **35**(3), 182–192 (2019).
68. Flanagan, T. P., Letendre, K., Burnside, W. R., Fricke, G. M. & Moses, M. E. Quantifying the effect of colony size and food distribution on harvester ant foraging. *PloS one* **7**(7), e39427 (2012).
69. Moses, M. E., Cannon, J. L., Gordon, D. M. & Forrest, S. Distributed adaptive search in T cells: lessons from ants. *Frontiers in immunology* **10**, 1357 (2019).

Acknowledgements

We thank the University of New Mexico Center for Advanced Research Computing, supported in part by NSF, for high-performance computing resources, as well as the James S. McDonnell Foundation and NSF awards 2030037 and 2020247 for funding. Thanks to Chris Kempes, Sid Redner, Alan Friedman, and the Moses Computational Biology Lab for the helpful discussions and reviews of earlier versions of this manuscript.

Author contributions

JF wrote the software and performed computational experiments under the supervision of GMF and MEM. JF, GMF, and MEM wrote the manuscript and created the figures. JLC supervised JF on the selection of simulation parameters, active immune response times in humans and mice, and helped the authors place our results in context. JF compiled published lymphoid tissue measurements under the supervision of MEM. JF derived the mathematical expressions under the supervision of GMF and MEM. All conceptual content and implementations are entirely generated by the authors. The paper was drafted entirely by the authors, and we used ChatGPT in a few instances to clarify or shorten individual sentences. For example, we asked ChatGPT to rewrite this sentence: "It has been unclear what drives a trade-off between LN size and number" ChatGPT produced: "The trade-off between LN size and number remains unexplained." This was done to edit approximately 5% of the paper.

Declarations

Competing interests

We declare we do not have any competing interests.

Additional information

Supplementary Information The online version contains supplementary material available at https://doi.org/10.1038/s41598-025-28443-2.

Correspondence and requests for materials should be addressed to J.F.

Reprints and permissions information is available at www.nature.com/reprints.

Publisher's note Springer Nature remains neutral with regard to jurisdictional claims in published maps and institutional affiliations.